Model-Based Detection of Heart Rate Turbulence Using Mean Shape Information

Danny Smith*, Kristian Solem, Pablo Laguna, *Senior Member, IEEE*, Juan Pablo Martínez, and Leif Sörnmo, *Senior Member, IEEE*

***Abstract*—A generalized likelihood ratio test (GLRT) statistic is proposed for detection of heart rate turbulence (HRT), where a set of Karhunen–Loève basis functions models HRT. The detector structure is based on the extended integral pulse frequency modulation model that accounts for the presence of ectopic beats and HRT. This new test statistic takes *a priori* information regarding HRT shape into account, whereas our previously presented GLRT detector relied solely on the energy contained in the signal subspace. The spectral relationship between heart rate variability (HRV) and HRT is investigated for the purpose of modeling HRV "noise" present during the turbulence period, the results suggesting that the white noise assumption is feasible to pursue. The performance was studied for both simulated and real data, leading to results which show that the new GLRT detector is superior to the original one as well as to the commonly used parameter turbulence slope (TS) on both types of data. Averaging ten ventricular ectopic beats, the estimated detection probability of the new detector, the previous detector, and TS were found to be 0.83, 0.35, and 0.41, respectively, when the false alarm probability was held fixed at 0.1.**

***Index Terms*—ECG, generalized likelihood ratio test (GLRT), heart rate turbulence (HRT), integral pulse frequency modulation (IPFM) model, Karhunen–Loève basis functions.**

I. Introduction

HEART rate turbulence (HRT) refers to a short-term fluctuation in heart rate triggered by a single ventricular ectopic beat (VEB) [1], [2]. Such turbulence is considered to be a blood-pressure-regulating mechanism, which, in normal subjects, compensates for the VEB-induced drop in blood pressure by an accelerated sinus rate. The heart rate then decelerates to its baseline level and the blood pressure returns to its preextrasystolic level [3]–[7]. In normal subjects, the presence of HRT can be detected and characterized provided that ensemble averaging of the RR interval series is first performed to improve the low SNR. The HRT magnitude depends on heart rate such that higher heart rates are coupled to lower magnitudes and *vice versa* [8]. Blunted or missing turbulence reflects autonomic dysfunction and is associated with various conditions. In particular, HRT has been established as a powerful risk predictor of mortality and sudden cardiac death following acute myocardial infarction [1], [2]. It has also been assessed and found useful for other patients including those with congestive heart failure [3], diabetes mellitus [3], and hypotension in hemodialysis patients [9].

To date, turbulence slope (TS) and turbulence onset (TO) are the two most commonly employed parameters for assessing HRT. The parameter TO measures the relative change in the RR intervals that enclose a VEB, defined by the relative difference of the averages of the two normal RR intervals before and after the VEB. The parameter TS quantifies the sinus deceleration that follow the VEB and is defined by the steepest slope observed over five consecutive RR intervals in the first 15 RR intervals following the VEB. A nonnegative value of TO or a low value of TS indicates that HRT is blunted or missing. It has been demonstrated that TS suffers from certain shortcomings, notably that TS is overestimated when few VEBs are available for averaging or when considerable heart rate variability (HRV) is present [10].

Several other parameters have been suggested in the literature for the purpose of characterizing HRT, although having received much less attention in clinical studies. These parameters include combined analysis of TO and TS [4], a TS-related parameter adjusted with respect to either heart rate or the number of averaged VEBs [10], turbulence timing, which indicates the first beat number from where TS is calculated [11], and the correlation coefficient of the regression line fitted to the five RR intervals of TS [12].

The parameters of the aforementioned HRT analysis are determined from an averaged RR interval tachogram, obtained by first aligning RR intervals that enclose the VEBs of a recording and then performing averaging. As a result, the computed parameter values provide a global characterization of the recording, usually acquired during 24 h, but precludes information on possible HRT dynamics. While averaging has proven to be useful in many clinical studies, it suffers nonetheless from the limitation of combining HRTs that may occur at different heart rates, and thus, have different turbulence shapes. Consequently, the assumption inherent to ensemble averaging of a signal shape being fixed throughout the recording may not always be valid. It would, of course, be desirable to introduce some technique for noise reduction that makes it possible to accurately

Manuscript received January 8, 2009; revised May 22, 2009 and July 9, 2009. First published August 25, 2009; current version published January 20, 2010. This work was supported by the Swedish Research Council, Gambro AB, Lund, Sweden, CICYT (TEC2007-68076-C02-02), and the Grupo Consolidado T30, DGA, Spain. *Asterisk indicates corresponding author.*

*D. Smith is with the Signal Processing Group, Department of Electrical and Information Technology, Lund University, and Center of Integrative Electrocardiology, Lund University (CIEL), 22100 Lund, Sweden (e-mail: danny.smith@eit.lth.se).

K. Solem was with the Department of Electrical and Information Technology, Lund University, Lund 22100, Sweden. He is now with Gambro Lundia AB, SE-220 10 Lund, Sweden.

P. Laguna and J. P. Martínez are with the Communications Technology Group, Aragón Institute for Engineering Research (I3A), University of Zaragoza, 50018 Zaragoza, Spain and also with the CIBER de Bioengeniería, Biomateriales y Nanomedicina (CIBER-BBN), 50018 Zaragoza, Spain.

L. Sörnmo is with the Signal Processing Group, Department of Electrical and Information Technology, Lund University, and Center of Integrative Electrocardiology at Lund University (CIEL), 22100 Lund, Sweden.

Digital Object Identifier 10.1109/TBME.2009.2030669

characterize each individual HRT, or at least when few VEBs need to be averaged. A step in this direction was recently taken in an interesting study done by Rojo-Álvarez *et al.* [13], where support vector machine estimation was exploited for the purpose of denoising individual HRTs. The parameter TS was computed on different types of datasets before and after denoising, leading to the conclusion that such denoising made analysis possible even when few VEBs were available.

Another approach to combatting noise in HRTs was recently presented where model-based, statistical detection was considered in relation to the integral pulse frequency modulation (IPFM) model, but extended to account for HRT [14]. It was assumed that the observed signal can be viewed as the summation of HRV, modeled by additive white Gaussian noise, and HRT, modeled as a linear combination of Karhunen–Loève (KL) basis functions. An advantage with that detector is that the observations are indexed with time rather than with beat occurrence, which is inherent to the tachogram, and thereby that approach is better matched to physiology and will compensate for the fact that TS leads to structural correlation between HRT and heart rate [10]. While the resulting test statistic of the generalized likelihood ratio test (GLRT) is primarily used to decide whether HRT is present or not, its magnitude reflects HRT strength and may therefore be used as a descriptive parameter as well. Results from simulated data suggested that the GLRT detector offers better performance than does TS since at least twice the number of VEBs for averaging are needed for TS to attain a performance, which is identical to that of the GLRT detector [14].

The assumption of HRV being modeled as white noise is clearly unrealistic as it contradicts the well-known fact that the HRV spectrum has a certain structure that reflects autonomic balance [15]. This assumption was still considered because it does not require power spectral estimation and leads to a detector with simple structure [14]. In the present paper, the white noise assumption is examined in terms of HRV and HRT power spectra and its feasibility for modeling HRV is considered. Following the work published in [14], it was found that the assumption of HRT being modeled as an unrestricted linear combination of basis functions sometimes lead to turbulence shapes that have nonphysiological characteristics, i.e., the signal model is not restricted to the acceleration–deceleration response that is usually referred to as a turbulence shape. In order to solve this problem, a revised model is presented here, where certain *a priori* information on turbulence shape is incorporated; the corresponding GLRT detector is derived and evaluated. The present study includes a performance evaluation that goes much beyond the one in [14]: first, detection performance is now evaluated when the turbulence shape is allowed to vary, and, second, a large dataset of ECGs with or without HRT is studied for evaluation purposes.

This paper is organized as follows. Section II presents the datasets used for investigating the white noise assumption and evaluating the HRT detector, including both simulated RR interval data and long-term ECG recordings. The spectral properties of HRV and HRT are analyzed in Section III in order to shed light on the noise modeling assumption. Section IV describes the new detector that incorporates information on mean turbulence shape, and the subsequent section presents its performance and compares it to that of the GLRT detector in [14] as well as to that of TS. A discussion of the method and its performance is found in Section VII.

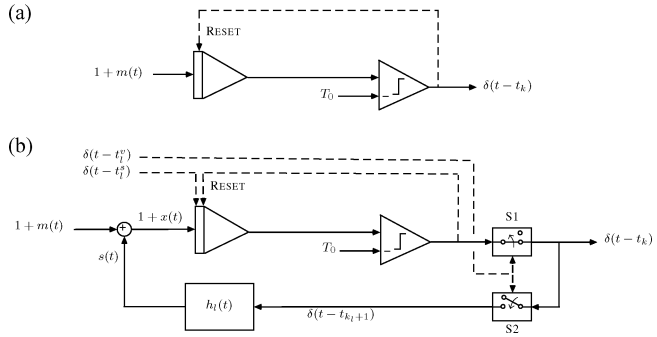

Fig. 1. Block diagram of (a) original IPFM model and (b) extended IPFM model. The two switches S1 and S2 are positioned such that normal sinus rhythm is modeled. The dashed lines describe control signals.

II. MATERIALS

A. Simulated Signals Using the Extended IPFM Model

The IPFM model can be used to create a series of heartbeat occurrence times from a continuous-time modulating signal $m(t)$, which reflects the autonomic influence on the cardiac rhythm [15]. An extended IPFM model was recently proposed that accounts for HRT by introducing a feedback branch that is triggered by an ectopic beat (see Fig. 1) [14]. An additive approach is used where the input signal $x(t)$ to the model is given by the sum of the HRT signal $s(t)$ and the HRV signal $m(t)$. The deterministic signal $s(t)$ is the sum of all turbulence episodes

$$s(t) = \sum_{l=1}^{N_e} h_l(t - t_{k_l+1}) \tag{1}$$

where $h_l(t)$ is the turbulence response to the lth VEB and N_e denotes the number of VEBs. The occurrence time for the first normal beat after the lth VEB is denoted t_{k_l+1}. The HRV signal $m(t)$ is usually viewed as physiological, but is, in this context, viewed as observation noise. Moving to a discrete-time representation, the observations $\mathbf{x}_l$ of the lth VEB can be written as

$$\mathbf{x}_l = \mathbf{h}_l + \mathbf{m}_l \tag{2}$$

where $\mathbf{h}_l$ and $\mathbf{m}_l$ are the $N \times 1$ discrete-time vectors of HRT and HRV, respectively. The HRT response to the lth VEB is modeled linearly with a truncated set of KL basis functions

$$\mathbf{h}_l = \mathbf{B}\boldsymbol{\theta}_l \tag{3}$$

where $\mathbf{B}$ is an $N \times r$ matrix whose r columns contain the KL basis functions, and $\boldsymbol{\theta}_l$ is an $r \times 1$ vector containing the KL coefficients associated with the lth VEB. The basis functions in $\mathbf{B}$ together with $\boldsymbol{\theta}_l$ define the turbulence shape.

In this study, the output of the extended IPFM model is considered for evaluation of detector performance, being based on

the assumption that the HRT response $\mathbf{h}_l$ is fixed and deterministic. The matrix $\mathbf{B}$ is determined from the observations of some representative ECG dataset, and its columns are defined by the most significant eigenvectors of the average correlation matrix $\bar{\mathbf{R}}_{\mathbf{x}}$ of equidistantly resampled observations $\mathbf{x}_l$ containing turbulence. The vector $\mathbf{m}_l$ accounting for HRV is generated by a seventh-order autoregressive (AR) model, representing variability during resting conditions [14]. The desired SNR between HRV and HRT is obtained by changing the ratio between the energy of $\mathbf{h}_l$ and $\mathbf{m}_l$.

B. ECG Signals

The long-term ST database contains 86 ECG Holter recordings of 80 subjects, acquired during clinical routine in the U.S. and Europe [16]. The recordings are 2- or 3-lead of up to 24 h duration and sampled at 250 Hz with 12-bit resolution. Each recording was manually annotated, including information on ectopy. A VEB was discarded from further analysis if any of the following criteria was fulfilled for the surrounding RR intervals [2].

1) An RR interval is $<$300 or $>$2000 ms.
2) The difference in length between two adjacent RR intervals is $>$200 ms.
3) $>$20% difference to a reference RR interval defined as the average of the five sinus intervals preceding the VEB.
4) The coupling interval is $>$80% of the average RR in ten sinus beats preceding the VEB.
5) The compensatory pause is $<$120% of the average RR in ten sinus beats preceding the VEB.
6) The distance between successive VEBs is $<$30 s; this criterion ensures that HRTs do not influence each other.

These criteria ensure that the sinus rhythm immediately preceding and following the VEB is free of artefacts, arrhythmia, and false classifications, and thus, suitable for HRT analysis.

1) Dataset for Spectral Study: When analyzing the spectral properties of HRT and HRV (see Section III), following two additional criteria were introduced.

1) The recording should contain $\geq$40 VEBs to ensure that the variance of the spectral estimate is significantly reduced through averaging.
2) TS $<$15 so that outlier HRTs are excluded from further analysis.

Application of these two additional criteria together with the previous six criteria resulted in a total of 3498 VEBs from 22 recordings.

2) Datasets for Detector Evaluation: When evaluating detector performance on ECG data (see Section VI), the following two datasets were used: one containing recordings with HRT, denoted $\mathcal{S}_1$, and another without HRT, denoted $\mathcal{S}_0$. A recording was included in $\mathcal{S}_1$ if it contained $\geq$15 VEBs, which all complied with the previous six criteria and with a TS $>$ 2.5. Due to the low SNR of a single VEB, TS is considered reliable if at least 15 VEBs has been averaged prior to estimation. Application of these two additional criteria together with the previous six criteria resulted in a total of 5764 VEBs from 26 recordings. The set $\mathcal{S}_0$ is constructed by extracting 26 577 segments from ten patients without any VEBs. The set $\mathcal{S}_1$ is randomly divided into a learning set ($\mathcal{S}_{1,l}$) and a test set ($\mathcal{S}_{1,t}$), whereas the whole dataset $\mathcal{S}_0$ is used for testing.

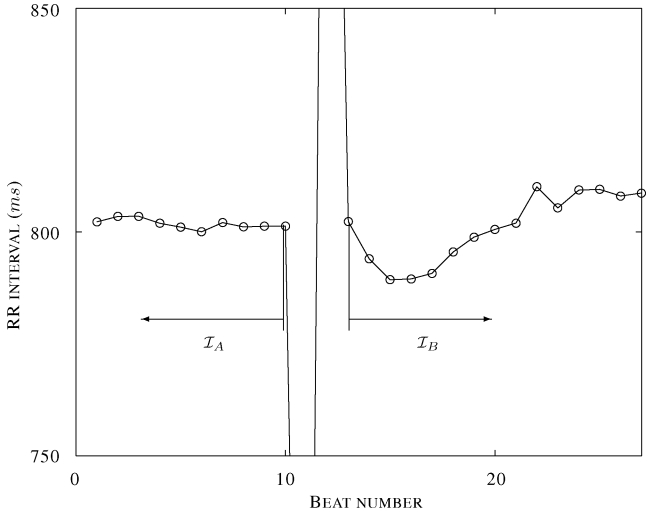

Fig. 2. Segment definition for the RR interval tachogram containing a VEB. Segment $\mathcal{I}_A$ contains 15 s of normal RR intervals that precede the VEB, whereas $\mathcal{I}_B$ contains 15 s of RR intervals that are subsequent to the VEB.

III. Spectral Properties of HRV and HRT

The purpose of this section is to analyze the spectral properties of HRV and HRT in order to support the assumptions made later on concerning the observation model. The analysis also provides some insight on the SNR for these two activities. Our approach lies in comparing power spectra estimated from the segments located just before and after a VEB, respectively. The following frequency bands are studied: the low-frequency (LF) band 0.04–0.15 Hz, the high-frequency (HF) band 0.15–0.40 Hz, and the LF+HF frequency band 0.04–0.40 Hz.

A. Spectral Relationships for HRV and HRT

The segments located just before and after a VEB are denoted $\mathcal{I}_A$ and $\mathcal{I}_B$, respectively, and both contain the RR intervals occurring during 15 s of normal sinus rhythm (see Fig. 2). Thus, $\mathcal{I}_A$ contains HRV only, whereas $\mathcal{I}_B$ may contain both HRV and HRT.

The parameter ΔP can be viewed as a measure of the increase in power following a VEB. This parameter is defined as the difference between the average power spectrum $\bar{P}_A(e^{j\omega})$ and $\bar{P}_B(e^{j\omega})$, resulting from the $\mathcal{I}_A$ and $\mathcal{I}_B$ segments, respectively, and normalized with the power of $\bar{P}_A(e^{j\omega})$

$$\Delta P = \frac{\int_{\omega_1}^{\omega_2} (\bar{P}_B(e^{j\omega}) - \bar{P}_A(e^{j\omega}))d\omega}{\int_{\omega_1}^{\omega_2} \bar{P}_A(e^{j\omega})d\omega} \tag{4}$$

where ω_1 and ω_2 define the different frequency bands mentioned earlier. The average power spectrum $\bar{P}(e^{j\omega})$ is obtained by estimating the power spectrum $\hat{P}_l(e^{j\omega})$ for each $\mathcal{I}_A$ or $\mathcal{I}_B$ segment

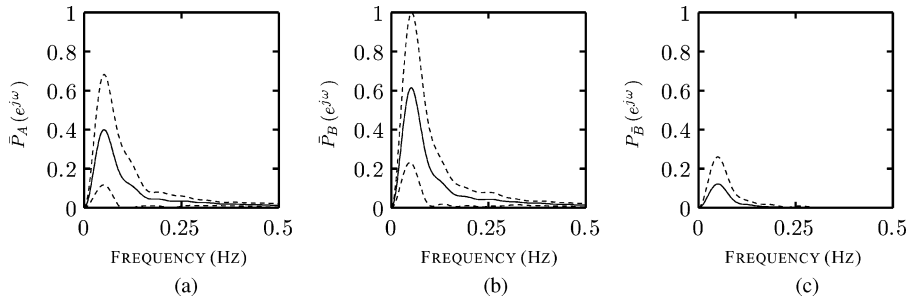

Fig. 3. Average power spectra reflecting (a) HRV, (b) combined influence of HRV and HRT, and (c) HRT, respectively. One standard deviation is displayed for each power spectrum using dashed lines.

and then averaging, we have

$$\bar{P}(e^{j\omega}) = \frac{1}{N_e}\sum_{l=1}^{N_e}\hat{P}_l(e^{j\omega}) \tag{5}$$

where N_e denotes the number of VEBs in a record. In this study, a power spectrum $\hat{P}_l(e^{j\omega})$ is estimated using the periodogram

$$\hat{P}_l(e^{j\omega}) = \frac{1}{N}|X_l(e^{j\omega})|^2 \tag{6}$$

where $X_l(e^{j\omega})$ is the discrete-time Fourier transform of an N-point vector $\mathbf{x}_l$, based on data from either $\mathcal{I}_A$ or $\mathcal{I}_B$ segments, with its mean value removed and padded with zeros to always become a 1024-point vector. Averaging of a sufficiently large number of vectors $\mathbf{x}_l$ estimated from $\mathcal{I}_B$ segments will cancel HRV and produce an estimate of HRT; the segment with averaged data is denoted $\mathcal{I}_{\bar{B}}$. An estimate of the SNR in terms of HRT and HRV is given by the ratio between the power in the $\mathcal{I}_{\bar{B}}$ segment (HRT) and the power in the $\mathcal{I}_B$ segment (the sum of HRV and HRT) after subtracting the power in the $\mathcal{I}_{\bar{B}}$ segment (HRT),

$$\eta_{\mathrm{SNR}} = \frac{\int_{\omega_1}^{\omega_2} P_{\bar{B}}(e^{j\omega})d\omega}{\int_{\omega_1}^{\omega_2} \bar{P}_B(e^{j\omega})d\omega - \int_{\omega_1}^{\omega_2} P_{\bar{B}}(e^{j\omega})d\omega} \tag{7}$$

where ω_1 and ω_2 are the frequencies defining the LF+HF band.

B. Spectral Observations

Fig. 3 shows the average power spectra for segments $\mathcal{I}_A$, $\mathcal{I}_B$, and $\mathcal{I}_{\bar{B}}$ when HRT is present. It is evident that $\bar{P}_A(e^{j\omega})$, $\bar{P}_B(e^{j\omega})$, and $P_{\bar{B}}(e^{j\omega})$ overlap spectrally. It is also evident that the power spectra computed before and after a VEB are similar in shape, but not in magnitude.

Fig. 4 shows that the total power of $\bar{P}_B(e^{j\omega})$ increases as the turbulence level increases in relation to $\bar{P}_A(e^{j\omega})$ as does the power in LF band. However, there is much less activity in the HF band, thus indicating that HRT is mostly confined to the LF band. This result agrees with the knowledge that HRT is a blood pressure regulating function [1], being characterized by a spectral peak around 0.1 Hz [15]. As expected, the estimated SNR increases as TS increases (see Fig. 5). Based on the entire set of VEBs, the mean TS was computed and found to be 5.1 ms per beat that corresponds to an SNR of $\eta_{\mathrm{SNR}} = -9.0$ dB. Such a low SNR clearly indicates that HRV is still very present during HRT and accounts for most of the power contained in a single $\mathcal{I}_B$ segment.

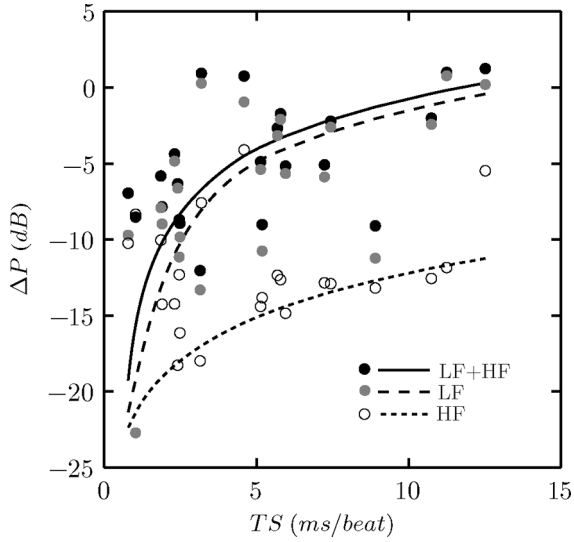

Fig. 4. Power ratio ΔP as a function of TS [cf., the definition in (4)] for the LF, HF, and LF+HF bands. Robust line fitting is used to facilitate interpretation of the data.

These observations show that a substantial spectral overlap exists between $\mathcal{I}_A$ and $\mathcal{I}_B$ segments. Since the HRT spectrum $P_{\bar{B}}(e^{j\omega})$ is largely confined inside the HRV spectrum $\bar{P}_A(e^{j\omega})$, a noise whitening operation would also whiten the HRT signal and render detection improvement difficult. It is, therefore, concluded that white noise assumption is feasible to adopt in a model for HRT detection, which is shown shortly.

IV. METHODS

Our previously proposed detector, presented in [14], was based on the extended IPFM model and an equidistantly sampled signal $\mathbf{x}_l$, obtained after the lth VEB in a recording. Dropping the index l, the detection problem was formulated as

$$\begin{aligned}\mathcal{H}_0 &: \quad \mathbf{x} = \mathbf{m} \\ \mathcal{H}_1 &: \quad \mathbf{x} = \mathbf{B}\boldsymbol{\theta} + \mathbf{m}\end{aligned} \tag{8}$$

where hypothesis $\mathcal{H}_0$ represents when HRT is absent and hypothesis $\mathcal{H}_1$ when present. The $N \times 1$ observation vector $\mathbf{x}$ is obtained from the RR intervals according to the method described in [14], $\mathbf{m}$ is an $N \times 1$ vector and represents HRV, here treated as random observation noise. The $N \times r$ matrix $\mathbf{B}$ contains r different KL basis functions that model HRT, cf. (3), and

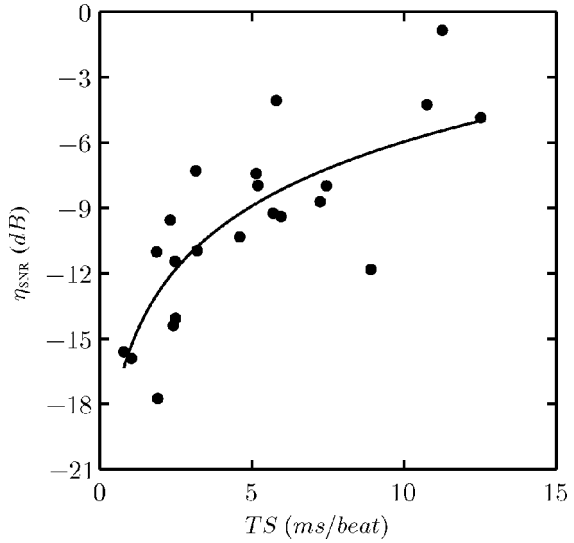

Fig. 5. Estimated SNR η_{SNR} for HRT and HRV as a function of TS [cf., the definition in (7)]. Robust line fitting is used to facilitate interpretation of the data.

the vector $\boldsymbol{\theta}$ is a deterministic $r \times 1$ vector with unknown KL coefficients.

The related GLRT test statistic, denoted $T_\theta(\mathbf{x})$, was used to decide hypothesis $\mathcal{H}_1$ if [14]

$$T_\theta(\mathbf{x}) = \frac{N-r}{r} \frac{\hat{\boldsymbol{\theta}}^T \hat{\boldsymbol{\theta}}}{\mathbf{x}^T\mathbf{x} - \hat{\boldsymbol{\theta}}^T \hat{\boldsymbol{\theta}}} > \gamma' \tag{9}$$

where

$$\hat{\boldsymbol{\theta}} = \mathbf{B}^T\mathbf{x} \tag{10}$$

is the KL coefficient estimator and γ' an appropriately chosen threshold. The energy projected on the signal space (spanned by the r basis functions) is given by $\mathbf{x}^T\mathbf{B}\mathbf{B}^T\mathbf{x}$, whereas the energy projected on the orthogonal $(N-r)$-dimensional noise space is given by $\mathbf{x}^T(\mathbf{I} - \mathbf{B}\mathbf{B}^T)\mathbf{x}$. As a result, the test statistic $T_\theta(\mathbf{x})$ can be viewed as an estimate of the SNR that reflects the ratio between HRT and HRV [14].

The detector $T_\theta(\mathbf{x})$ suffers from the disadvantage of relying solely on energy, accepting all HRT shapes defined by the signal subspace even if they are not physiological. Our approach to solve this limitation is to introduce *a priori* information about the shape of HRT in terms of the vector $\boldsymbol{\mu}$, which contains the KL coefficients of the mean turbulence shape. Exchanging the unknown vector $\boldsymbol{\theta}$ for the known $\boldsymbol{\mu}$ leads to the following model

$$\begin{aligned} \mathcal{H}_0 &: \quad \mathbf{x} = \mathbf{m} \\ \mathcal{H}_1 &: \quad \mathbf{x} = \mathbf{B}\boldsymbol{\mu} + \mathbf{m} \end{aligned} \tag{11}$$

where, as before, $\mathcal{H}_0$ represents when HRT is absent and $\mathcal{H}_1$ when present. The vector $\boldsymbol{\mu}$ is an $r \times 1$ vector containing the KL coefficients of the mean turbulence shape that is estimated *a priori* from a learning set. Based on the observations made in Section III, HRV is characterized by the Gaussian probability density function (pdf) $\mathcal{N}(\mathbf{0}, \sigma^2\mathbf{I})$, where $\mathbf{I}$ denotes the identity matrix and σ^2 the variance, which, here, is assumed to be unknown, and therefore, subjected to estimation.

The related detector is based on the Neyman–Pearson theorem in which the probability of detection P_{D} is maximized for a given probability of false alarm $P_{\mathrm{FA}} = \alpha$ by deciding $\mathcal{H}_1$ if [17]

$$L(\mathbf{x}) = \frac{p(\mathbf{x};\mathcal{H}_1)}{p(\mathbf{x};\mathcal{H}_0)} > \gamma \tag{12}$$

where $p(\mathbf{x};\mathcal{H}_i)$ denotes the PDF of $\mathbf{x}$ under $\mathcal{H}_i$, and the threshold γ is found from

$$P_{\mathrm{FA}} = \int_{\{\mathbf{x}:L(\mathbf{x})>\gamma\}} p(\mathbf{x};\mathcal{H}_0)\, d\mathbf{x} = \alpha. \tag{13}$$

Using the signal model in (11) and the Neyman–Pearson theorem, the GLRT becomes

$$L_G(\mathbf{x}) = \frac{p(\mathbf{x};\hat{\sigma}^2_{\mathcal{H}_1},\mathcal{H}_1)}{p(\mathbf{x};\hat{\sigma}^2_{\mathcal{H}_0},\mathcal{H}_0)} > \gamma \tag{14}$$

where $\hat{\sigma}^2_{\mathcal{H}_i}$ is the maximum-likelihood (ML) estimate of σ^2, assuming that $\mathcal{H}_i$ is true.

If we let

$$T_\mu(\mathbf{x}) = L_G(\mathbf{x})^{2/N} > \gamma^{2/N} = \gamma' \tag{15}$$

which is a monotonically increasing function of $L_G(\mathbf{x})$, and therefore, an equivalent test statistic, then we can define (see the Appendix for derivation)

$$T_\mu(\mathbf{x}) = \frac{\mathbf{x}^T\mathbf{x}}{(\mathbf{x}-\mathbf{B}\boldsymbol{\mu})^T(\mathbf{x}-\mathbf{B}\boldsymbol{\mu})} > \gamma' \tag{16}$$

where the resulting test statistic $T_\mu(\mathbf{x})$ of the GLRT in (14) is used for HRT detection. Hypothesis $\mathcal{H}_1$ is decided if $T_\mu(\mathbf{x}) > \gamma'$, where γ' is a threshold determined for a given P_{FA}. The detector statistic $T_\mu(\mathbf{x})$ can be viewed as the ratio of the squared Euclidean distance between $\mathbf{x}$ and the origin, and the distance between $\mathbf{x}$ and $\mathbf{B}\boldsymbol{\mu}$. The expectation of $\mathbf{x}$ when HRT is absent or present is 0 or $\mathbf{B}\boldsymbol{\mu}$, respectively [cf., (11)]. Hence, $T_\mu(\mathbf{x})$ will be close to zero when HRT is absent and increase when HRT is present.

V. Detector Evaluation

In the detector evaluation, the GLRT detectors use basis functions that resulted from $\mathcal{S}_{1,l}$, (i.e., $\mathbf{B} = \hat{\mathbf{B}}_l$), whereas the extended IPFM simulation model use basis functions that resulted from $\mathcal{S}_{1,t}$, $(\mathbf{B} = \hat{\mathbf{B}}_t)$. Both $\hat{\mathbf{B}}_l$ and $\hat{\mathbf{B}}_t$ are obtained as the three most significant eigenvectors (i.e., $r = 3$) of two average correlation matrices $\bar{\mathbf{R}}_x$ estimated from the observations $\mathbf{x}_l$ of the two sets $\mathcal{S}_{1,t}$ and $\mathcal{S}_{1,l}$. Each observation $\mathbf{x}_l$ is 10 s, resulting in a 21×1 vector. The mean shape vector $\boldsymbol{\mu}$ also differed from model to detector (described shortly) to avoid the risk of producing simulated signals that are matched to the detectors.

Evaluation of detector performance using different SNRs was performed using the simulator model. The model employed a mean shape resulting from $\mathcal{S}_{1,t}$ $(\boldsymbol{\mu} = \hat{\boldsymbol{\mu}}_t)$, whereas the detector employed a mean shape resulting from $\mathcal{S}_{1,l}$, $(\boldsymbol{\mu} = \hat{\boldsymbol{\mu}}_l)$. A total of 4000 signals were simulated for each of the evaluated SNRs, divided in 2000 signals with HRT and 2000 without.

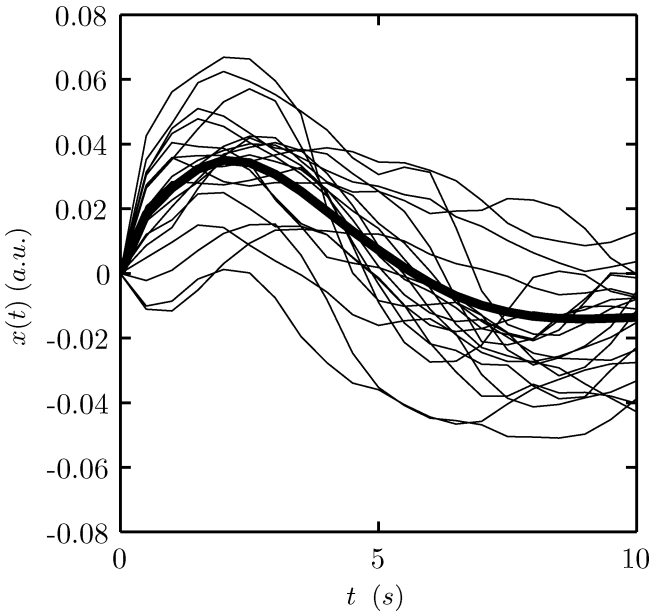

Fig. 6. Mean turbulence shape $\boldsymbol{\mu}$ (thick line) and 20 averaged observations $\bar{\mathbf{x}}$ ($N_e = 10$), obtained from $\mathcal{S}_{1,l}$. Note that $x(t)$ in this diagram is inversely proportional to the commonly displayed RR interval tachogram.

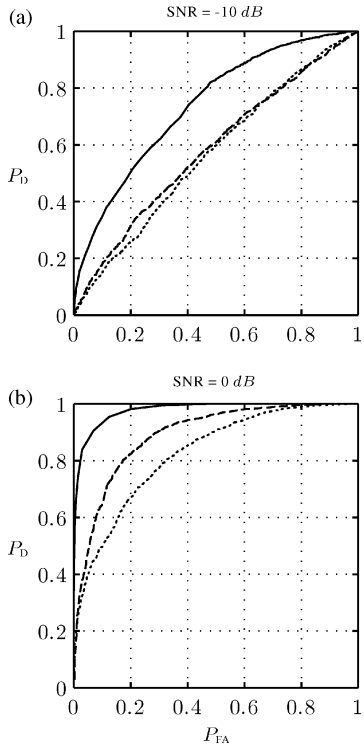

Fig. 7. ROCs for $T_\mu(\mathbf{x})$ (solid line), $T_\theta(\mathbf{x})$ (dashed line), and TS (dotted line) when analyzing simulated signals. The performance is evaluated at an SNR of (a) -10 dB and (b) 0 dB.

In order to evaluate how variations in mean shape affects detection performance, simulations were performed where the model uses a set of varying mean shapes to generate signals. A set of M vectors $\tilde{\boldsymbol{\mu}}_i$ were produced

$$\tilde{\boldsymbol{\mu}}_i = \hat{\boldsymbol{\mu}}_t + \Delta\boldsymbol{\mu}_i, \qquad i = 1, \ldots, M \tag{17}$$

where the vectors $\Delta\boldsymbol{\mu}_i$ accounts for the variability ($M = 100$). Generation of $\Delta\boldsymbol{\mu}_i$ is accomplished by producing a random vector $\mathbf{u}_i \sim \mathcal{N}(\mathbf{0}, \sigma_\mu^2\mathbf{I})$ of size $1 \times r$, which is multiplied with the Cholesky decomposition of the covariance matrix estimated from the KL coefficients calculated from dataset S_1, thus producing a set of generated KL coefficients. Due to a low SNR between HRV and HRT, σ_μ is used as a scaling factor in order to ensure that the generated vectors $\tilde{\boldsymbol{\mu}}_i$ resembles HRT. Setting $\sigma_\mu = 0.25$ resulted in a variety of turbulence shapes with physiological appearance.

Further, detection performance was evaluated on ECG signals using the datasets $\mathcal{S}_0$ and $\mathcal{S}_{1,t}$. It should be noted that VEB averaging is not required in GLRT detection, but the test statistic $T_\mu(\mathbf{x})$ can just as well be evaluated for single VEBs. If averaging is considered, the observation vector $\mathbf{x}$ is replaced with $\bar{\mathbf{x}}$ in the test statistic, being the ensemble average of $\mathbf{x}_l$, $l = 1, 2, \ldots, N_e$. Fig. 6 shows the mean turbulence shape resulting from the learning set $\mathcal{S}_{1,l}$ as well as examples of averaged observations $\bar{\mathbf{x}}$.

VI. Results

Fig. 7(a) presents the receiver operating characteristics (ROCs) for $T_\mu(\mathbf{x})$, $T_\theta(\mathbf{x})$, and TS at a very low SNR (-10 dB) of the simulated signals, showing that $T_\mu(\mathbf{x})$ performs better than both $T_\theta(\mathbf{x})$ and TS. At this SNR, the performance of the latter two detectors is random as the ROCs essentially coincide with the diagonal, i.e., the performance is identical to the outcome of tossing a coin with heads and tails. Increasing the SNR to 0 dB, the difference in performance becomes more pronounced between the three detectors with $T_\mu(\mathbf{x})$ outperforming the other two [see Fig. 7(b)]. It should be noted that $T_\theta(\mathbf{x})$ performs better than does TS at this SNR. Fig. 7(b) shows that $T_\mu(\mathbf{x})$, $T_\theta(\mathbf{x})$, and TS attain detection probabilities (P_{D}) of 0.94, 0.65, and 0.50, respectively, at a false alarm probability (P_{FA}) of 0.1. For an SNR of 10 dB (not shown), the performances of all three detectors are essentially perfect, and therefore, it can be concluded that SNRs ranging from about -10 to 10 dB are of interest to study in simulations. The lower bound of this range roughly corresponds to the SNR of a single VEB as found in Section III-B.

Fig. 8 shows the detection performance for simulated signals when using 100 different mean shapes in the model at an SNR of 0 dB. Results are presented for the 10th, 50th, and 90th percentile of each detector. At a false alarm probability of $P_{\mathrm{FA}} = 0.1$ the probability of detection for $T_\mu(x)$ ranges from 0.64 to 0.96 with a median of 0.89 [see Fig. 8(a)], whereas $T_\theta(x)$ ranges from 0.39 to 0.73 with a median of 0.61 [see Fig. 8(b)] and TS from 0.30 to 0.63 with a median of 0.46 [see Fig. 8(c)]. $T_\mu(x)$ clearly offers better performance than do $T_\theta(x)$ and TS when variations in the mean shape are present.

Turning to the ECG signals, detector performance is evaluated on the test set $(\mathcal{S}_0, \mathcal{S}_{1,t})$, using parameters determined from the learning set $(\mathcal{S}_{1,l})$ (see Section V); details on the design of datasets are found in Section II-B. Applying the three detectors to single VEBs, i.e., without resorting to averaging, the ROCs in Fig. 9(a) show that $T_\mu(\mathbf{x})$ performs better than both $T_\theta(\mathbf{x})$ and TS. Increasing the SNR by averaging ten VEBs, it is obvious from Fig. 9(b) that $T_\mu(\mathbf{x})$ offers superior performance when compared to the other two detectors that are quite similar in

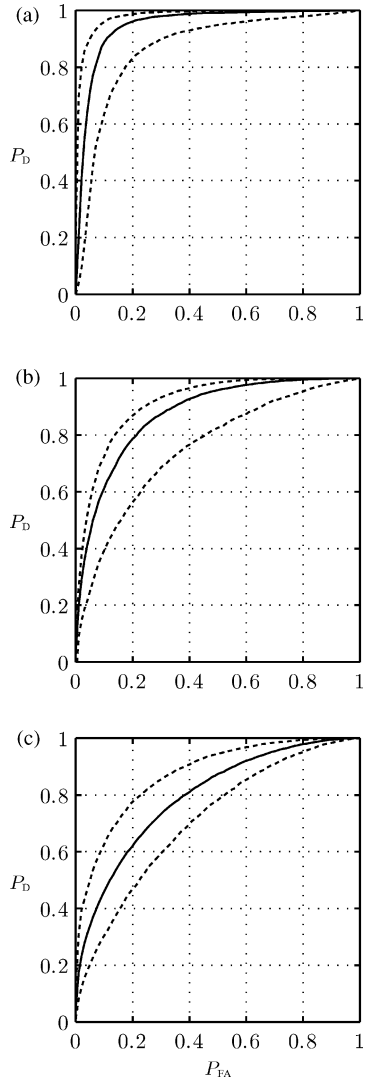

Fig. 8. ROCs obtained when evaluating performance on simulated signals generated using 100 different mean shapes. Solid line describes ROC for the 50th percentile, dashed lines for the 10th and 90th percentile for (a) $T_\mu(\mathbf{x})$, (b) $T_\theta(\mathbf{x})$, and (c) TS using an SNR of 0 dB.

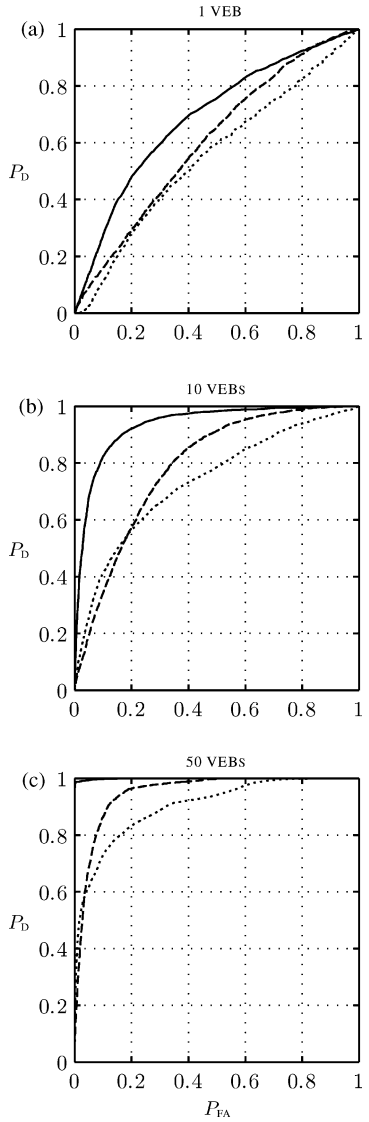

Fig. 9. ROCs for $T_\mu(\mathbf{x})$ (solid line), $T_\theta(\mathbf{x})$ (dashed line), and TS (dotted line) when analyzing ECG signals. The performance is evaluated for (a) single VEBs, (b) averaging of ten VEBs, and (c) averaging of 50 VEBs.

performance. The detection probabilities of $T_\mu(\mathbf{x})$, $T_\theta(\mathbf{x})$, and TS are found to be 0.83, 0.35, and 0.41, respectively, at $P_{\rm FA} = 0.1$. A further increase of the SNR, obtained by averaging 50 VEBs, results in an almost perfect ROC for $T_\mu(\mathbf{x})$ since $P_{\rm D} = 1$ for almost all values of $P_{\rm FA}$ [see Fig. 9(c)]. The performance of $T_\theta(\mathbf{x})$ and TS is still inferior with $P_{\rm D} = 0.86$ and $P_{\rm D} = 0.73$, respectively, at $P_{\rm FA} = 0.1$. Results have been summarized in Table I.

It is interesting to note that the ROCs resulting from simulations and ECG signals, displayed in Figs. 7 and 9, respectively, have a striking resemblance. Simulated signals with an SNR of -10 dB and ECG signals without VEB averaging have similar ROCs, as do simulated signals with an SNR of 0 dB and ECG signals with ten VEBs averaged.

TABLE I
PROBABILITY OF DETECTION ($P_{\rm D}$) AT A FIXED FALSE ALARM PROBABILITY ($P_{\rm FA}$) OF 0.1

SIMULATED SIGNALS			
SNR (dB)	$T_\mu(\mathbf{x})$	$T_\theta(\mathbf{x})$	TS
-10	0.37	0.19	0.15
0	0.94	0.65	0.50
10	≈ 1	≈ 1	≈ 1
SIMULATED SIGNALS USING A VARYING MEAN SHAPE ($SNR = 0\ dB$)			
	$T_\mu(\mathbf{x})$	$T_\theta(\mathbf{x})$	TS
median	0.89	0.61	0.46
ECG SIGNALS			
# VEB	$T_\mu(\mathbf{x})$	$T_\theta(\mathbf{x})$	TS
1	0.30	0.18	0.11
10	0.83	0.35	0.41
50	≈ 1	0.86	0.73

VII. DISCUSSION

In our previous work, HRV was treated as additive observation noise and modeled as white [14]. This assumption is

certainly unrealistic since the spontaneous variability in heart rate is correlated. However, we have shown in this paper that the spectral content of HRT is contained within the HRV spectrum (see Fig. 3), and thus, the white noise assumption seems feasible to use since a whitening procedure would whiten the HRV and HRT components similarly as well as requiring more parameters to be estimated. The results also show that HRV remains in play during HRT.

Introducing the mean turbulence shape $\boldsymbol{\mu}$, a large improvement in performance was found on both simulated and real signals when compared to the original GLRT detector $T_\theta(\mathbf{x})$ and the commonly used parameter TS. This improvement can be explained by the new detector being able to distinguish between physiological and nonphysiological turbulence, thereby leading to better detection accuracy. Evaluation of simulated data, generated using different mean shapes, showed that the new detector is robust and can handle variations in the turbulence shape while maintaining high accuracy. Another advantage compared to TS is that the detector uses equidistantly sampled observations as input, and therefore, does not suffer from structural correlation to heart rate that is inherent to beat-related measures [10].

In Section III-B, we made the observation that the mean TS is 5.1 ms per beat for a single VEB, corresponding to $\eta_{\mathrm{SNR}} = -9.0$ dB. As a result, an SNR of about 0 dB is achieved by averaging ten VEBs (an SNR gain of 3 dB is obtained when twice as many VEBs are averaged). The results for simulated signals using an SNR of -10 dB and evaluating the detector on single VEBs yield similar performance. This was also found for an SNR of 0 dB and ten averaged VEBs. Good detection performance is found when averaging ten VEBs, which for $T_\mu(\mathbf{x})$ gives a high probability of detection, while retaining a low probability of false alarm (see Fig. 9). In terms of SNR, $T_\mu(\mathbf{x})$ achieves excellent performance at an SNR of 0 dB.

The current GLRT statistic $T_\mu(\mathbf{x})$ estimates the variance σ^2 under both $\mathcal{H}_0$ and $\mathcal{H}_1$. A test statistic using a fixed variance was also investigated during the progress of this paper for which the variance was estimated *a priori* from the training set. While the resulting performance was almost at par with that obtained for running variance estimation, fixed variance would imply the use of a detector structure that needs more *a priori* information. This would lead to reduced generality when using the detector on other databases.

When constructing the dataset S_1, we relied on TS as a measure of HRT presence (see Section II), which to date is the clinically accepted method. A recording with a sufficient number of VEBs, where the averaged beat tachogram had $\mathrm{TS} > 2.5$, was included in the dataset, the assumption being that the average beat tachogram represents the HRT response after each VEB. There is likely a certain number of VEBs present in the HRT dataset that does not contain HRT, especially in the lower TS range (just above $\mathrm{TS} = 2.5$). This will affect the probability of detection negatively and the effect will be most visible when evaluating single or few averaged VEBs. The impact of this has not been studied since it will affect the evaluated detectors similarly.

Although $T_\mu(\mathbf{x})$ was found to perform very well for detection of HRT, further evaluation is needed to investigate if $T_\mu(\mathbf{x})$ can further improve the clinical significance of HRT. In particular, it is of crucial interest to study the present detector in terms of cardiac risk assessment, to date being the most successful application of HRT.

VIII. Conclusion

In this paper, the mean turbulence shape $\boldsymbol{\mu}$ was introduced in the signal model and the related GLRT detector was derived. The results show that $T_\mu(\mathbf{x})$ outperforms the previously proposed $T_\theta(\mathbf{x})$ and the commonly used parameter TS. This paper also showed that HRV, in this model considered to be observation noise, may be modeled using the white noise assumption. A heuristic connection between the SNR and the number of averaged VEBs was established where an SNR of 0 dB is roughly obtained by averaging ten VEBs.

Appendix

Derivation of the Test Statistic $T_\mu(\mathbf{x})$ From the GLRT in (14)

The GLRT in (14) decides $\mathcal{H}_1$ if

$$L_G(\mathbf{x}) = \frac{p(\mathbf{x}; \hat{\sigma}^2_{\mathcal{H}_1}, \mathcal{H}_1)}{p(\mathbf{x}; \hat{\sigma}^2_{\mathcal{H}_0}, \mathcal{H}_0)} > \gamma \tag{18}$$

where

$$p(\mathbf{x}; \sigma^2, \mathcal{H}_1) = \frac{1}{(2\pi\sigma^2)^{N/2}} \exp\left[-\frac{1}{2\sigma^2}(\mathbf{x} - \mathbf{B}\boldsymbol{\mu})^T(\mathbf{x} - \mathbf{B}\boldsymbol{\mu})\right] \tag{19}$$

and

$$p(\mathbf{x}; \sigma^2, \mathcal{H}_0) = \frac{1}{(2\pi\sigma^2)^{N/2}} \exp\left[-\frac{1}{2\sigma^2}\mathbf{x}^T\mathbf{x}\right]. \tag{20}$$

The MLE of σ^2 under $\mathcal{H}_1$ and $\mathcal{H}_0$ is found by maximizing $p(\mathbf{x}; \sigma^2, \mathcal{H}_1)$ and $p(\mathbf{x}; \sigma^2, \mathcal{H}_0)$, respectively, over σ^2

$$\hat{\sigma}^2_{\mathcal{H}_1} = \frac{1}{N}(\mathbf{x} - \mathbf{B}\boldsymbol{\mu})^T(\mathbf{x} - \mathbf{B}\boldsymbol{\mu}) \tag{21}$$

$$\hat{\sigma}^2_{\mathcal{H}_0} = \frac{1}{N}\mathbf{x}^T\mathbf{x}. \tag{22}$$

Hence

$$p(\mathbf{x}; \hat{\sigma}^2_{\mathcal{H}_1}, \mathcal{H}_1) = \frac{1}{\left(2\pi\hat{\sigma}^2_{\mathcal{H}_1}\right)^{N/2}} \exp\left[-\frac{N}{2}\right] \tag{23}$$

and

$$p(\mathbf{x}; \hat{\sigma}^2_{\mathcal{H}_0}, \mathcal{H}_0) = \frac{1}{\left(2\pi\hat{\sigma}^2_{\mathcal{H}_0}\right)^{N/2}} \exp\left[-\frac{N}{2}\right]. \tag{24}$$

Thus, the GLRT is

$$L_G(\mathbf{x}) = \left(\frac{\hat{\sigma}^2_{\mathcal{H}_0}}{\hat{\sigma}^2_{\mathcal{H}_1}}\right)^{N/2} > \gamma. \tag{25}$$

If we let

$$T_\mu(\mathbf{x}) = L_G(\mathbf{x})^{2/N} > \gamma^{2/N} = \gamma' \tag{26}$$

which is a monotonically increasing function of $L_G(\mathbf{x})$, and therefore, an equivalent test statistic, then we can

define

$$T_\mu(\mathbf{x}) = \frac{\hat{\sigma}^2_{\mathcal{H}_0}}{\hat{\sigma}^2_{\mathcal{H}_1}} = \frac{\mathbf{x}^T\mathbf{x}}{(\mathbf{x}-\mathbf{B}\boldsymbol{\mu})^T(\mathbf{x}-\mathbf{B}\boldsymbol{\mu})} > \gamma'. \quad (27)$$

REFERENCES

[1] G. Schmidt, M. Malik, P. Barthel, R. Schneider, K. Ulm, L. Rolnitzky, A. J. Camm, J. T. Bigger, and A. Schömig, "Heart-rate turbulence after ventricular premature beats as a predictor of mortality after acute myocardial infarction," *Lancet*, vol. 353, pp. 1390–1396, 1999.

[2] R. Schneider, P. Barthel, and M. Watanabe, "Heart rate turbulence on Holter," in *Dynamic Electrocardiography*, M. Malik and A. J. Camm, Eds. New York: Futura, 2004, ch. 20, pp. 190–193.

[3] M. Watanabe and G. Schmidt, "Heart rate turbulence: A 5-year review," *Heart Rhythm*, vol. 1, pp. 732–738, 2004.

[4] M. Watanabe, "Heart rate turbulence: A review," *Indian Pacing Electrophysiol. J.*, vol. 3, pp. 10–22, 2003.

[5] S. Raj, R. Sheldon, M. Koshman, and D. Roach, "Role of hypotension in turbulence physiology," *Heart Rhythm*, vol. 2, pp. 710–717, 2005.

[6] M. Watanabe, "Role of hypotension in heart rate turbulence," *Heart Rhythm*, vol. 2, pp. 828–829, 2005.

[7] A. Bauer and G. Schmidt, "Last piece of the heart rate turbulence puzzle?" *Heart Rhythm*, vol. 4, pp. 290–291, 2007.

[8] A. Bauer, M. Malik, P. Barthel, R. Schneider, M. Watanabe, A. Camm, A. Schömig, and G. Schmidt, "Turbulence dynamics: An independent predictor of late mortality after acute myocardial infarction," *Int. J. Cardiol.*, vol. 107, pp. 42–47, 2006.

[9] K. Solem, A. Nilsson, and L. Sörnmo, "An electrocardiogram-based method for early detection of abrupt changes in blood pressure during hemodialysis," *ASAIO J.*, vol. 52, pp. 282–290, 2006.

[10] A. Hallstrom, P. Stein, R. Schneider, M. Hodges, G. Schmidt, and K. Ulm, "Structural relationships between measures based on heart beat intervals: Potential for improved risk assessment," *IEEE Trans. Biomed. Eng.*, vol. 51, no. 8, pp. 1414–1420, Aug. 2004.

[11] M. Watanabe, J. Marine, R. Sheldon, and M. Josephson, "Effects of ventricular premature stimulus coupling interval on blood pressure and heart rate turbulence," *Circulation*, vol. 106, pp. 325–330, 2002.

[12] G. Schmidt, R. Schneider, and P. Barthel, "Correlation coefficient of the heart rate turbulence slope: New risk stratifier in post-infarction patients," *Eur. Heart J.*, vol. 22, p. 72, 2001 (P484).

[13] J. Rojo-Álvarez, O. Barquero-Pérez, I. Mora-Jiménez, E. Everss, A. Rodrígez-González, and A. García-Alberola, "Heart rate turbulence denoising using support vector machines," *IEEE Trans. Biomed. Eng.*, vol. 56, no. 2, pp. 310–319, Feb. 2009.

[14] K. Solem, P. Laguna, J. Martinez, and L. Sörnmo, "Model-based detection of heart rate turbulence," *IEEE Trans. Biomed. Eng.*, vol. 55, no. 12, pp. 2712–2722, 2008.

[15] L. Sörnmo and P. Laguna, *Bioelectrical Signal Processing in Cardiac and Neurological Applications*. Amsterdam, The Netherlands/New York: Elsevier/Academic, 2005.

[16] F. Jager, A. Taddei, G. B. Moody, M. Emdin, G. Antolic, R. Dorn, A. Smrdel, C. Marchesi, and R. G. Mark, "Long-term ST database: A reference for the development and evaluation of automated ischaemia detectors and for the study of the dynamics of myocardial ischaemia," *Med. Biol. Eng. Comput.*, vol. 41, no. 2, pp. 172–183, 2003.

[17] S. M. Kay, *Fundamentals of Statistical Signal Processing, Vol. II: Detection Theory*. Upper Saddle River, NJ: Prentice-Hall, 1998.

Danny Smith received the M.Sc. degree in information and communication engineering technologies in 2005 from Lund University, Lund, Sweden, where he is currently working toward the Ph.D. degree in signal processing and its application to biomedical signals.

His current research interests include ECG and photoplethysmography (PPG) signals and their significance in heart rate turbulence analysis and hemodialysis. He is also involved in teaching courses in signal processing.

Kristian Solem received the M.Sc. degree in electrical engineering and the Ph.D. degree in biomedical signal processing from Lund University, Lund, Sweden, in 2003 and 2008, respectively.

He is currently in the Research Department, Gambro Lundia AB, Lund. His current research interests include ECG, pressure, and photoplethysmography (PPG) signals and their significance in heart rate variability analysis, heart rate turbulence analysis, and hemodialysis.

Pablo Laguna (M'92–SM'06) was born in Jaca, Spain, in 1962. He received the M.S. degree in physics and the Ph.D. degree in physic science from the Science Faculty, University of Zaragoza, Zaragoza, Spain, in 1985 and 1990, respectively.

He is currently a Full Professor of signal processing and communications in the Department of Electrical Engineering, Engineering School, University of Zaragoza, where he is also a Researcher at the Aragón Institute for Engineering Research (I3A), where from 1992 to 2005, he was an Associate Professor. From 1987 to 1992, he was an Assistant Professor of automatic control in the Department of Control Engineering, Politecnic University of Catalonia (UPC), Spain, and as a Researcher at the Biomedical Engineering Division, Institute of Cybernetics (UPC-CSIC). He is also with the Networking Biomedical Research Centro de Investigacíon Biomédica en Red en Bioingeniería, Biomateriales y Nanomedicina (CIBER-BBN), Zaragoza. His current research interests include signal processing, in particular applied to biomedical applications. He is the author of the book *Bioelectrical Signal Processing in Cardiac and Neurological Applications* (Elsevier, 2005)

Juan Pablo Martínez was born in Zaragoza, Aragón, Spain, in 1976. He received the M.S. degree in telecommunication engineering and the Ph.D. degree in biomedical engineering from the University of Zaragoza (UZ), Zaragoza, in 1999 and 2005, respectively.

Since 2000, he has been an Assistant Professor at the Aragón Institute of Engineering Research, UZ, where he has been an Associate Professor since 2007. He is also with the Centro de Investigación Biomédica en Red en Bioingeniería, Biomateriales y Nanomedicina (CIBER-BBN). His current research interests include biomedical signal processing, with main interest in signals of cardiovascular origin.

Leif Sörnmo (S'77–M'84–SM'02) received the M.Sc. and Ph.D. degrees in electrical engineering from Lund University, Lund, Sweden, in 1978 and 1984, respectively.

From 1983 to 1995, he was engaged in problems in computer-based ECG analysis in the Department of Clinical Physiology, Lund University, where since 1990, he has been with the Signal Processing Group, Department of Electrical and Information Technology, and is currently a Professor in biomedical signal processing. His current research interests include statistical signal processing and modeling of biomedical signals, methods for atrial fibrillation analysis, multimodal signal processing in hemodialysis, detection of otoacoustic emissions, and power-efficient signal processing in implantable devices. He is the author of the book *Bioelectrical Signal Processing in Cardiac and Neurological Applications* (Elsevier, 2005). He has been an Associate Editor of the *Computers in Biomedical Research* (1997–2000). He is currently an Associate Editor of the *Journal of Electrocardiology*, and a member of the Editorial Board of the *Medical and Biological Engineering and Computing*.

Dr. Sörnmo is currently an Associate Editor of the IEEE TRANSACTIONS ON BIOMEDICAL ENGINEERING.